

Quadriexcitons and excitonic condensate in a symmetric electron-hole bilayer with valley degeneracy

Stefania De Palo,^{1,2,*} F. Tramonto,^{2,†} Saverio Moroni,^{1,3,‡} and Gaetano Senatore^{2,§}

¹*CNR-IOM-DEMOCRITOS, Trieste, Italy*

²*Dipartimento di Fisica, Università di Trieste, strada Costiera 11, 34151 Trieste, Italy*

³*SISSA (International School for Advanced Studies), via Bonomea 265, 34136 Trieste, Italy*

(Dated: April 22, 2022)

Using quantum Monte Carlo simulations we have mapped out the zero temperature phase diagram of a symmetric electron-hole bilayer with twofold valley degeneracy, as function of the interlayer distance d and in-layer density n . We find that the effect of the valley degeneracy is to shrink the region of stability of the excitonic condensate, in favor of quadriexcitons at small d and of the four-component plasma at large d , with minor effects on the value of the excitonic condensate fraction. The enclosure of the condensate in a density window possibly explains why anomalous tunnelling conductivity, interpreted as signature of condensation, is observed only between two finite values of carrier density in graphene bilayers. Our phase diagram may provide directions to select device parameters for future experiments.

The idea that spatially separated electrons and holes provide an ideal playground for the observation of superfluidity/superconductivity was put forward long ago [1]. An equilibrium condensate, however, has long remained elusive in conventional electron-hole semiconductor bilayers [2–4], while it was observed in semiconductor electron-electron (hole-hole) bilayers [5–7] in strong perpendicular magnetic fields [8], i.e., in the quantum Hall regime. It was recently argued that excitonic condensation should be strongly enhanced in coupled electron-hole graphene bilayers, where extremely thin hBN barriers can be used [9] and electrons and holes have equal masses. Yet, carrier valley degeneracy is present in graphene bilayers and its effect is not immediately obvious; moreover, (i) BCS mean field [10] would suggest an enhancement of the condensate, (ii) the screening by a larger number of Fermion components would point to a weakening of the e-h attraction, and (iii) the presence of four Fermion components in each bilayer would allow for the formation of quadriexcitons. [11].

Experiments on coupled graphene bilayers promptly followed the proposal in Ref. 9, replicating however the scenario encountered in semiconductor bilayers, with no evidence of a condensate in coupled electron-hole graphene bilayers [12, 13] and a clear evidence of a condensate in coupled electron-electron graphene bilayers in the quantum Hall regime [14, 15]. Eventually, evidence of condensed interbilayer excitons in zero magnetic field, signaled by enhanced tunneling, was reported in coupled electron-hole graphene bilayers [16] and more recently in coupled monolayers of transition metal dichalcogenides [17, 18]; moreover, thermodynamic evidence of the condensate was also provided [19]. We should recall at this point that some evidence of condensation was also found in semiconductor electron bilayers, with long lived indirect excitons produced by photoexcitation and electrostatic trapping [20, 21] and in excitons coupled to light confined within a cavity (exciton-polaritons), which do live long enough to condense and require a continuous input of light [22].

Here, we restrict to equilibrium excitonic condensation in

systems of electron and holes and assess the effects of the interplay of the valley degeneracy g_v , the interlayer distance d and the in-layer density n in determining the $T = 0$ phase diagram of the system. To this end we resort to QMC simulations of the simplest possible model, i.e., a paramagnetic, symmetric electron-hole bilayer ($m_e = m_h = m_b$, $g_v = 2$), to mimic the situation encountered in double bilayer graphene. In effective Hartree atomic units ($\hbar = m_b = e^2/(4\pi\epsilon_0\epsilon) = 1$), which we use throughout, the Hamiltonian of the system reads

$$\begin{aligned}
 H = & -\frac{1}{2} \sum_{v,i} \nabla_{e,v,i}^2 + \frac{1}{2} \sum'_{v,v',i,i'} \frac{1}{|\mathbf{r}_{e,v,i} - \mathbf{r}_{e,v',i'}|} \\
 & -\frac{1}{2} \sum_{v,i} \nabla_{h,v,i}^2 + \frac{1}{2} \sum'_{v,v',i,i'} \frac{1}{|\mathbf{r}_{h,v,i} - \mathbf{r}_{h,v',i'}|} \\
 & - \sum_{v,v',i,i'} \frac{1}{\sqrt{|\mathbf{r}_{e,v,i} - \mathbf{r}_{h,v',i'}|^2 + d^2}}, \quad (1)
 \end{aligned}$$

where terms with both $v' = v$ and $i' = i$ are excluded from the primed sums and $\mathbf{r}_{e,v,i}$ ($\mathbf{r}_{h,v,i}$) is the in-plane position of the i th electron (hole) in valley v . Above, m_b is the band effective mass of the carriers, which move in a medium of dielectric constant ϵ . QMC simulations of the $g_v = 1$ case are already available both at $T = 0$ [23–27] and at $T > 0$ [28].

At given valley degeneracy, the properties of the system depend on the interlayer distance d and the in-layer coupling parameter $r_s = 1/\sqrt{\pi n}$, while the ratio r_s/d measures the importance of the interlayer attraction, as compared to the in-layer repulsion. Provided that screening is not too strong, i.e., $r_s \gtrsim 1$, a paired phase is expected for $r_s/d > 1$ [23, 25]. Moreover, for $r_s/d \gg 1$ quadriexcitons [11] should appear, instead of the biexcitons found in the one valley case [25]. In this Letter we systematically investigate the region $r_s < 8$, for systems with $N = 84$ particles per layer. We also study some systems with a larger number of particles, up to $N = 148$, to assess size effects, as well as some systems at lower densities (larger r_s values).

We have employed variational and diffusion Monte Carlo [29–31] (VMC and DMC) as implemented in our own code.

At each r_s and d , an optimal trial function Ψ_T is determined by minimizing the variational energy with respect to a number of optimizable parameters [32]. We then compute estimates of the properties of interest using Monte Carlo integration with $|\Psi_T|^2$ as *importance function* and, in most cases, using also the more accurate fixed-node DMC[29, 30] with Ψ_T as guiding function. We have used a singlet BCS-Jastrow trial function [23, 33]

$$\Psi_T = J \prod_{\sigma} D_{e,h}^{\sigma,\sigma}, \quad (2)$$

$$D_{e,h}^{\sigma,\sigma} = \det[\phi(\mathbf{r}_{e,\sigma,i} - \mathbf{r}_{h,\sigma,j})], \quad (3)$$

with $\sigma = (v, s_z)$ the valley-spin index or flavor, and the Jastrow factor

$$J = \exp[-(1/2) \sum_{\mu,\mu'} \sum_{i_\mu,j_{\mu'}} u_{\mu,\mu'}(|\mathbf{r}_{i_\mu} - \mathbf{r}_{j_{\mu'}}|)] \quad (4)$$

embodying two-body correlations. Above, the *species* index $\mu = (t, \sigma)$ combines the particle type ($t = e, h$) and the flavor; moreover, the primed sum for $\mu' = \mu$ contains only the terms with $i_\mu \neq j_{\mu'}$. The pairing orbital $\phi(\mathbf{r})$ is chosen of a flexible form suggested earlier [25, 34],

$$\phi(\mathbf{r}) = c(r) + \sum_{l=1}^{N_k} p_{|\mathbf{k}_l|} \cos(\mathbf{k}_l \cdot \mathbf{r}), \quad (5)$$

where $c(r)$ is a spherical function of finite range $r_c \leq L/2$, L is the side of the periodic square simulation box, and the sum is over closed shells of the shortest reciprocal space wavevectors. The BCS part of the wavefunction $\prod_{\sigma} D_{e,h}^{\sigma,\sigma}$ is able to describe different homogeneous fluid phases [25]. When $p_{|\mathbf{k}_l|} = 0$ for all l one obtains a fluid of excitons. On the contrary when $c(r) = 0$, $N_k = N/4$ and $p_{|\mathbf{k}_l|} \neq 0$ for all l one obtains a plasma phase described by plane-wave Slater determinants. In this latter case, in fact, $D_{e,h}^{\sigma,\sigma} = D_e^{\sigma} D_h^{\sigma}$ [33] and $D_t^{\sigma} = \det[\exp(i\mathbf{k}_l \cdot \mathbf{r}_{t,\sigma,i})]$. The Jastrow factor, embodying two-body terms, apart from generally improving the wavefunction, is crucial in making possible polyexcitonic phases[35].

The function $c(r)$ and all pseudopotentials $u_{\mu,\mu'}(r)$ in the Jastrow factor are expanded on a flexible basis of locally piecewise-quintic Hermite interpolants [36], which among other things easily accommodates constraints at the end points. For each function its radial range and the expansion coefficients provide the variational parameters. For the pairing orbital $\phi(r)$ such a set of variational parameter is augmented by the plane wave coefficients $p_{|\mathbf{k}_l|}$. Depending on the chosen numbers of knots in the radial mesh and plane wave coefficients, the overall number of variational parameters used in the simulations describes below is typically between about 50 and 60. [37]

The main outcomes of our DMC simulations are summarized in the phase diagram displayed in Fig.1(a). For small values of the intralayer coupling $r_s \lesssim 1$ (large density), a four-component plasma phase is found stable at all distances

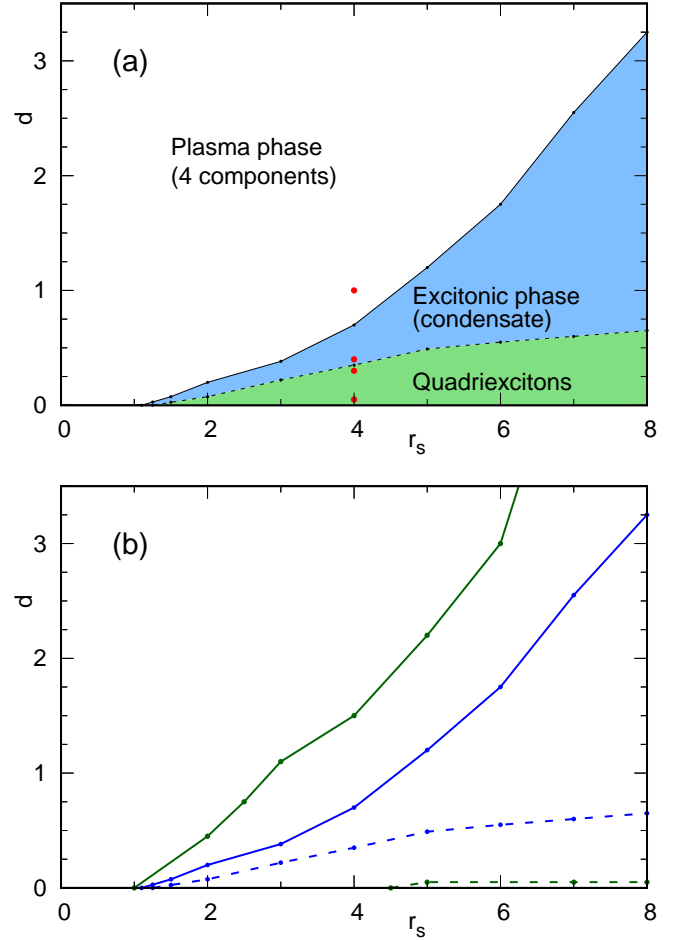


FIG. 1. (a) Phase diagram of an electron-hole bilayer with twofold valley degeneracy for small to moderate values of the intralayer coupling r_s and interlayer distance d . The red dots indicate states that are studied in Figs. 2 and 3. The regions of stability of the competing (fluid) phases are displayed in different colors. (b) Comparison of the phase diagrams of electron-hole bilayers with one and two valleys. The region of stability of the excitonic condensate in the one-valley system (area between the green lines [25, 38]) is substantially reduced in going to the two-valley system (area between the blue lines).

evidently due to strong screening. As one turns to larger values of r_s ($r_s \gtrsim 1$) the interlayer attraction becomes more effective and stabilizes a novel quadriexcitonic phase at smaller distances and an excitonic phase with condensate at intermediate distances. As illustrated in Fig.1(b), with respect to the findings of DMC simulations for a symmetric electron-hole bilayer without valley degeneracy [23, 25] we obtain a substantial shrinking of the region of stability of the excitonic phase, especially at small r_s . This may partly explain the difficulties encountered in finding experimental evidence of excitonic condensation in coupled electron-hole graphene bilayers [12, 13, 16] and suggests avoiding high density in the search of the condensate, as has been noted before [9]. In the density range investigated here, we find no evidence of

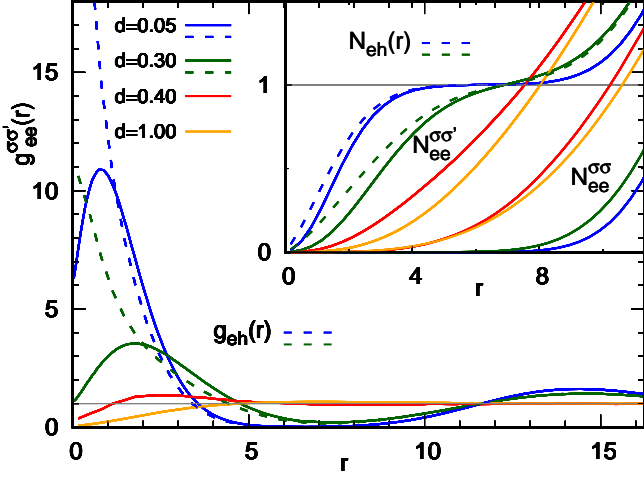


FIG. 2. PCFs (full lines) between electrons (holes) with different flavors ($\sigma' \neq \sigma$) in a symmetric electron-hole bilayer with twofold valley degeneracy, at $r_s = 4$; interlayer distances d correspond to various phases (see Fig 1). The inset reports the RCNs defined in Eq. 6. Electron-hole PCFs and RCNs are also shown for the two smaller distances (dashed lines), where they turn out to be independent of flavors, which have therefore been dropped.

biexcitons[25], which appear to be substituted by the much more stable quadriexcitons [39]. Below we characterize the various phases by analyzing features of the extrapolated estimates of pair correlation functions and condensate fraction [37].

In Fig. 2 we report the pair correlation function (PCF) [37] between electrons with different flavor $g_{ee}^{\sigma\sigma'}(r)$, $\sigma' \neq \sigma$, at $r_s = 4$. By symmetry, $g_{ee}^{\sigma\sigma'}(r) = g_{hh}^{\sigma\sigma'}(r)$. In the plasma phase ($d = 1$) the PCF is structureless for $r \gtrsim 5$, with a modest correlation hole for $r \lesssim 5$. In the excitonic phase ($d = 0.4$) the PCF remains structureless at larger distances, though showing a modest increase at smaller distances. As one crosses into the quadriexcitonic phase ($d = 0.3$) a large peak (higher than 3) appears at small distances, followed by a deep wide minimum, inducing pronounced oscillations at large distances. This behavior, is further enhanced at $d = 0.05$ with a peak as large as 11 and a minimum of 0. So, what is causing an "effective attraction" between unlike flavor electrons (holes), that overcomes direct Coulomb repulsion and produces such a short-range ordering? We note that this phenomenon is accompanied by the fact that the electron-hole PCF $g_{eh}^{\sigma\sigma'}(r)$, which is strongly peaked on the electron, become independent on the flavor and display the same deep wide minimum found in $g_{ee}^{\sigma\sigma'}(r)$, $\sigma' \neq \sigma$. A clue to what is going on is provided by the inspection of the distance-dependent pile-up of particles of the species (t', σ') around a particle of the species (t, σ), i.e., the running coordination number (RCN)

$$N_{tt'}^{\sigma\sigma'}(r) = 2\pi n_{t',\sigma'} \int_0^r ds s g_{tt'}^{\sigma\sigma'}(s), \quad (6)$$

$n_{t,\sigma}$ being a species areal density.

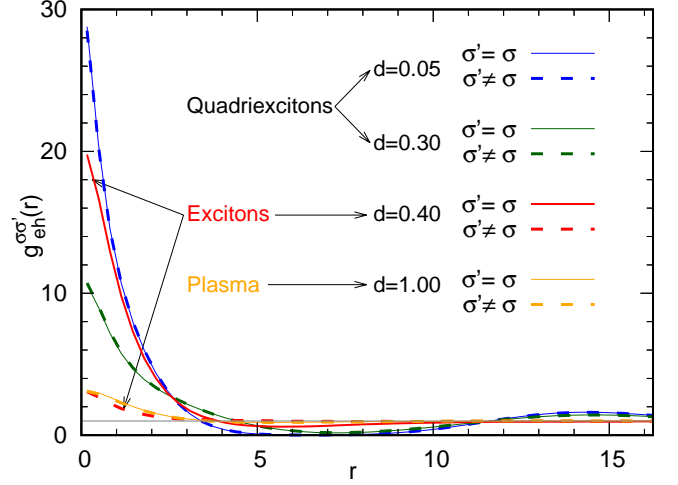


FIG. 3. Electron-hole PCFs in a symmetric electron-hole bilayer with twofold valley degeneracy, at $r_s = 4$ and interlayer distances d corresponding to various phases (see Fig 1). The PCFs of quadriexcitons and plasma are independent of flavors σ, σ' .

In the inset of Fig. 2 we display $N_{ee}^{\sigma\sigma'}(r)$ and $N_{eh}^{\sigma\sigma'}(r)$, respectively counting the average number of electrons (holes) with flavor σ' around an electron with flavor σ . Let us consider the case $d = 0.05$ first. It is evident that electrons with the same flavor as the one at the origin are completely expelled from a very large region, $N_{ee}^{\sigma\sigma}(r) \simeq 0$, $r \lesssim 8$. They make space for a dynamic compound of radius about 5, comprising 4 electrons (the one at the origin and 3 with $\sigma' \neq \sigma$) and 4 holes of the four flavors. This is what we call quadriexciton. At $d = 0.05$ the quadriexciton appears to be well defined, being neatly separated by its nearest neighbors, whereas at $d = 0.30$ neighboring quadriexcitons touch and at $d = 0.40$ they are melted into excitons.

The comparison in Fig. 3 of the electron-hole PCFs of the various phases at $r_s = 4$ reveals in the excitonic phase a large difference between paired ($\sigma' = \sigma$) and unpaired ($\sigma' \neq \sigma$) $g_{eh}^{\sigma\sigma'}(r)$, the height at the origin differing by as much as a factor 6. On the contrary, $g_{eh}^{\sigma\sigma}(r)$ is flavor independent both in the plasma phase, a consequence of the symmetry of the wavefunction, and in the quadriexcitonic phase, seemingly as an effect of the interplay of pseudopotentials and pairing orbital in the energy minimization. Such an interplay often results in a very repulsive pseudopotential $u_{\mu,\mu}(r)$ between electrons (holes) with the same flavor, as found also in the biexcitonic phase of the one-valley system [25]. We remark that the qualitative features of PCFs and RCNs of the various phases illustrated above for $r_s = 4$ are common to the whole density range displayed in Fig.1.

The condensate fraction n_0/n in the excitonic phase is shown in Fig. 4 for $r_s = 5$, as function of the interlayer distance d [37]. Comparison of the present results with those for the one-valley system [25] reveals that valley degeneracy, while substantially reducing the region of stability of the excitonic phase, leaves essentially unchanged the value of the

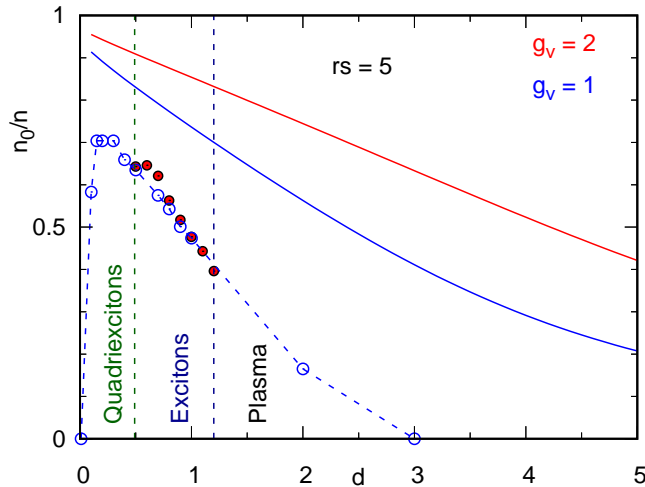


FIG. 4. Condensate fraction versus interlayer distance d in a symmetric electron-hole bilayer, at $r_s = 5$: (a) present results for $g_v = 2$ (red dots), with vertical dashed lines providing boundaries between phases; (b) $g_v = 1$ [25] (blue circles), with the dashed blue line a guide to the eyes; (c) BCS mean field [10] predictions (full curves).

condensate fraction. On the other hand, comparison with the predictions of a BCS treatment [10], uncovers the limitations of such a mean-field approach, which predicts for the condensate a substantial increase with valley degeneracy and a much slower decay with the distance d . The results at $r_s = 5$ are representative of our findings in the full range of density investigated in the present work, i.e., $r_s \leq 8$, when one keeps in mind that (i) the stability window (in distance) of the excitonic phase grows with r_s , as it is clear from Fig. 1, and (ii) the condensate fraction becomes somewhat smaller than in the one-valley system at large densities ($r_s < 3$).

The excitonic condensate at $T = 0$ may be found in three regimes [40]: BCS at high density, BEC at low density and BCS-BEC crossover in the middle. In order to characterize the regime for given d and r_s one may use the values of the condensate fraction n_0/n [27, 41] and $k_F r_{ex}$ [42], the ratio of the exciton radius r_{ex} and the interexciton distance $\sim 1/k_F$, k_F being the Fermi wavevector of electrons. The exciton radius is evaluated as

$$r_{ex}^2 = 2\pi n_{h,\sigma} \int_0^{r_1} ds s g_{eh}^{\sigma\sigma}(s) s^2, \quad (7)$$

with r_1 the radius of the circle centred on an electron containing on average one hole. In the density range studied here we find [37] $0.21 \leq n_0/n \leq 0.75$ and $0.31 \leq k_F r_{ex} \leq 0.96$ which, using the criteria of Refs. 27 and 41, places the condensate always in the BEC-BCS crossover regime.

We now turn to a peculiar aspect of the determination of the phase boundaries in Fig.1. The wavefunctions obtained through energy minimization display an hysteresis phenomenon when crossing a boundary. For the sake of clarity consider the quadriexciton to exciton transition at fixed r_s , which takes place at $d_{qe}(r_s)$ and choose $r_s = 4$, where

$d_{qe}(4) = 0.35$. If at $d \gtrsim 0.35$ we start the energy minimization with a converged quadriexcitonic wavefunction taken from $d < 0.35$ the wavefunction remains quadriexcitonic in character, with zero condensate. However, by increasing d further the wavefunction eventually becomes excitonic, with a finite condensate. Similarly, if at $d \lesssim 0.35$ we start with a converged excitonic wavefunction taken from $d > 0.35$ we find that the wavefunction remains excitonic; however if we decrease d further the wavefunction eventually becomes quadriexcitonic, with zero condensate. This implies that in the vicinity of $d = 0.35$ we have two solutions with different character and different VMC energies as well as fixed-node DMC energies. The latter more accurate energies are thus used to determine the stable phase near the boundary[37].

To conclude, we comment on the correspondence of the calculated phase diagram (Figs. 1) with interlayer conductance measurements in double-bilayer graphene-WSe₂ heterostructures[16]. In the experiment, a nominally divergent differential conductance between the two graphene bilayers, observed in a density interval (n_{\min}, n_{\max}) , is attributed to condensation of electron-hole pairs[16, 17, 43]. Suppression of condensation is ascribed to in-plane screening for $n > n_{\max}$ and to disorder or competing phases for $n < n_{\min}$, as generally expected for indirect excitons.[44, 45]. We can be more specific and relate the onset of pair condensation to phase transitions from plasma to excitons on the high density side, which is common to one-valley electron-hole devices[17, 25], and from quadriexcitons to excitons on the low density side, which represents a mechanism peculiar to two-valley devices even in the absence of disorder[46]. We note that the large extent of the quadriexcitonic phase, compared to the biexcitonic phase in the one-valley system[25], is instrumental in having suppression of pair condensation at low density for interlayer spacings accessible experimentally.

The experimental observation of condensation is strongly peaked around conditions of balanced electron and hole densities[16], matching the symmetric two-valley system considered here. Other aspects of our model, such as the assumption of parabolic bands[47] and isotropic dielectric constant, are less faithfully representative of the actual heterostructure. Nevertheless, using the largest and the smallest dielectric constants[16] of the constituent materials to translate device parameters to our units, the experimental spacing between graphene bilayers varies from 0.1 to 0.5. This is well within the region where we find a non-zero condensate bracketed by the plasma and the quadriexciton phases.

Our results support and complement measurements of interlayer tunneling conductance[16, 17, 43] as a probe for indirect exciton condensation.

* depalo@iom.cnr.it

† Present address: Kyndryl Italia Innovation Services S.r.l., Via Circonvallazione Idroscalo snc, 20090 Segrate (MI), Italy

- † moroni@iom.cnr.it
§ senatore@units.it
- [1] Y. E. Lozovik and V. I. Yudson, Feasibility of superfluidity of paired spatially separated electrons and holes; a new superconductivity mechanism, *JEPT Lett.* **22**, 274 (1975); A new mechanism for superconductivity: pairing between spatially separated electrons and holes, *Sov. Phys. JEPT* **44**, 389 (1976).
 - [2] U. Sivan, P. M. Solomon, and H. Shtrikman, Coupled electron-hole transport, *Phys. Rev. Lett.* **68**, 1196 (1992).
 - [3] A. F. Croxall, K. Das Gupta, C. A. Nicoll, M. Thangaraj, H. E. Beere, I. Farrer, D. A. Ritchie, and M. Pepper, Anomalous coulomb drag in electron-hole bilayers, *Phys. Rev. Lett.* **101**, 246801 (2008).
 - [4] J. A. Seamons, C. P. Morath, J. L. Reno, and M. P. Lilly, Coulomb drag in the exciton regime in electron-hole bilayers, *Phys. Rev. Lett.* **102**, 026804 (2009).
 - [5] M. Kellogg, J. P. Eisenstein, L. N. Pfeiffer, and K. W. West, Vanishing hall resistance at high magnetic field in a double-layer two-dimensional electron system, *Phys. Rev. Lett.* **93**, 036801 (2004).
 - [6] E. Tutuc, M. Shayegan, and D. A. Huse, Counterflow measurements in strongly correlated gaas hole bilayers: Evidence for electron-hole pairing, *Phys. Rev. Lett.* **93**, 036802 (2004).
 - [7] J. P. Eisenstein and A. H. MacDonald, Bose–einstein condensation of excitons in bilayer electron systems, *Nature* **432**, 691 (2004).
 - [8] Indeed, in an electron-electron bilayer at half filling in each layer, an electron-hole transformation in one of the two layers yields a compensated electron-hole bilayer [48].
 - [9] A. Perali, D. Neilson, and A. R. Hamilton, High-temperature superfluidity in double-bilayer graphene, *Phys. Rev. Lett.* **110**, 146803 (2013).
 - [10] X. Zhu, P. B. Littlewood, M. S. Hybertsen, and T. M. Rice, Exciton condensate in semiconductor quantum well structures, *Phys. Rev. Lett.* **74**, 1633 (1995).
 - [11] J. S.-Y. Wang and C. Kittel, Excitonic molecules: A possible new form of chemical bonding, *Physics Letters A* **42**, 189 (1972).
 - [12] J. I. A. Li, T. Taniguchi, K. Watanabe, J. Hone, A. Levchenko, and C. R. Dean, Negative coulomb drag in double bilayer graphene, *Phys. Rev. Lett.* **117**, 046802 (2016).
 - [13] K. Lee, J. Xue, D. C. Dillen, K. Watanabe, T. Taniguchi, and E. Tutuc, Giant frictional drag in double bilayer graphene heterostructures, *Phys. Rev. Lett.* **117**, 046803 (2016).
 - [14] X. Liu, K. Watanabe, T. Taniguchi, B. I. Halperin, and P. Kim, Quantum hall drag of exciton condensate in graphene, *Nat Phys* **13**, 746 (2017).
 - [15] J. I. A. Li, T. Taniguchi, K. Watanabe, J. Hone, and C. R. Dean, Excitonic superfluid phase in double bilayer graphene, *Nat Phys* **13**, 751 (2017).
 - [16] G. W. Burg, N. Prasad, K. Kim, T. Taniguchi, K. Watanabe, A. H. MacDonald, L. F. Register, and E. Tutuc, Strongly enhanced tunneling at total charge neutrality in double-bilayer graphene-wse₂ heterostructures, *Phys. Rev. Lett.* **120**, 177702 (2018).
 - [17] Z. Wang, D. A. Rhodes, K. Watanabe, T. Taniguchi, J. C. Hone, J. Shan, and K. F. Mak, Evidence of high-temperature exciton condensation in two-dimensional atomic double layers, *Nature* **574**, 76 (2019).
 - [18] The suggestion to resort to coupled monolayers of transition metal dichalcogenides was put forward in Ref. 49.
 - [19] L. Ma, P. X. Nguyen, Z. Wang, Y. Zeng, K. Watanabe, T. Taniguchi, A. H. MacDonald, K. F. Mak, and J. Shan, Strongly correlated excitonic insulator in atomic double layers, *Nature* **598**, 585 (2021).
 - [20] A. A. High, J. R. Leonard, M. Remeika, L. V. Butov, M. Hanson, and A. C. Gossard, Condensation of excitons in a trap, *Nano Letters* **12**, 2605 (2012), pMID: 22509898, <http://dx.doi.org/10.1021/nl300983n>.
 - [21] R. Anankine, M. Beian, S. Dang, M. Alloing, E. Cambril, K. Merghem, C. G. Carbonell, A. Lemaître, and F. Dubin, Quantized vortices and four-component superfluidity of semiconductor excitons, *Phys. Rev. Lett.* **118**, 127402 (2017).
 - [22] J. Kasprzak, M. Richard, S. Kundermann, A. Baas, P. Jeambrun, J. M. J. Keeling, F. M. Marchetti, M. H. Szymańska, R. André, J. L. Staehli, V. Savona, P. B. Littlewood, B. Deveaud, and L. S. Dang, Bose–einstein condensation of exciton polaritons, *Nature* **443**, 409 (2006).
 - [23] S. De Palo, F. Rapisarda, and G. Senatore, Excitonic condensation in a symmetric electron-hole bilayer, *Phys. Rev. Lett.* **88**, 206401 (2002).
 - [24] G. Senatore and S. D. Palo, Correlation effects in low dimensional electron systems: the electron?hole bilayer, *Contributions to Plasma Physics* **43**, 363 (2003).
 - [25] R. Maezono, P. López Ríos, T. Ogawa, and R. J. Needs, Excitons and biexcitons in symmetric electron-hole bilayers, *Phys. Rev. Lett.* **110**, 216407 (2013).
 - [26] R. O. Sharma, L. K. Saini, and B. P. Bahuguna, Ground state properties of electron-hole bilayer: Mass-asymmetric effect, *Phys. Rev. B* **94**, 205435 (2016).
 - [27] P. López Ríos, A. Perali, R. J. Needs, and D. Neilson, Evidence from quantum monte carlo simulations of large-gap superfluidity and bcs-bec crossover in double electron-hole layers, *Phys. Rev. Lett.* **120**, 177701 (2018).
 - [28] J. Schleele, A. Filinov, M. Bonitz, and H. Fehske, Phase diagram of bilayer electron-hole plasmas, *Contrib. Plasma Phys.* **52**, 819 (2012).
 - [29] P. J. Reynolds, D. M. Ceperley, B. J. Alder, and W. A. Lester, Fixed?node quantum monte carlo for molecules a) b), *The Journal of Chemical Physics* **77**, 5593 (1982).
 - [30] C. J. Umrigar, M. P. Nightingale, and K. J. Runge, A diffusion monte carlo algorithm with very small time?step errors, *J. Chem. Phys.* **99**, 2865 (1993), <https://doi.org/10.1063/1.465195>.
 - [31] W. M. C. Foulkes, L. Mitas, R. J. Needs, and G. Rajagopal, Quantum monte carlo simulations of solids, *Rev. Mod. Phys.* **73**, 33 (2001).
 - [32] We have used the linear method [50, 51] and checked, in selected cases, that the obtained minimum agrees with the one found by the improved stochastic reconfiguration method [52].
 - [33] Bouchaud, J.P., Georges, A., and Lhuillier, C., Pair wave functions for strongly correlated fermions and their determinantal representation, *J. Phys. France* **49**, 553 (1988).
 - [34] J. Carlson, S.-Y. Chang, V. R. Pandharipande, and K. E. Schmidt, Superfluid fermi gases with large scattering length, *Phys. Rev. Lett.* **91**, 050401 (2003).
 - [35] We have used 4 independent pseudopotentials $u_{\mu,\mu'}$, with appropriate cusp conditions [53]: same-flavor same-particle pairs, different-flavor same-particle pairs, same-flavor electron-hole pairs, and different-flavor electron-hole pairs. $\phi(r)$ is taken cusplless.
 - [36] V. Natoli and D. M. Ceperley, An optimized method for treating long-range potentials, *J. Comp. Phys.* **117**, 117 (1995).
 - [37] See the Supplemental Material at [URL] for details of the simulations, optimization across phase boundaries, estimate of the condensate fraction and structure of the quadriexcitons. The Supplemental material cites Refs. 23, 25, 54.
 - [38] The boundary between plasma and excitonic phases in the one-

- valley system (upper green line), is estimated from the values of the condensate fraction available on an (r_s, d) grid [25].
- [39] We have preliminary results indicating that by increasing the distance from $d=0$ an isolated quadriexciton would dissociate into two biexcitons at $d = 0.74$. By increasing the distance farther, at $d = 0.87$ biexcitons dissociates into excitons [55, 56]. In fact, with four flavors a dissociation of a quadriexciton into one triexciton and one exciton could also be possible.
- [40] A. J. Leggett, Diatomic molecules and cooper pairs, in *Modern Trends in the Theory of Condensed Matter*, edited by A. Pękalski and J. A. Przystawa (Springer Berlin Heidelberg, Berlin, Heidelberg, 1980) pp. 13–27.
- [41] A. Guidini and A. Perali, Band-edge BCS–BEC crossover in a two-band superconductor: physical properties and detection parameters, *Superconductor Science and Technology* **27**, 124002 (2014).
- [42] F. Pistolesi and G. C. Strinati, Evolution from bcs superconductivity to bose condensation: Role of the parameter $k_f \xi$, *Phys. Rev. B* **49**, 6356 (1994).
- [43] I. B. Spielman, J. P. Eisenstein, L. N. Pfeiffer, and K. W. West, Resonantly enhanced tunneling in a double layer quantum hall ferromagnet, *Phys. Rev. Lett.* **84**, 5808 (2000).
- [44] Comte, C. and Nozières, P., Exciton bose condensation : the ground state of an electron-hole gas - i. mean field description of a simplified model, *J. Phys. France* **43**, 1069 (1982).
- [45] P. B. Littlewood and X. Zhu, Possibilities for exciton condensation in semiconductor quantum-well structures, *Physica Scripta* **T68**, 56 (1996).
- [46] Quadriexciton condensation is also possible in principle, but we expect that enhanced mass, reduced density and interaction-induced depletion will strongly suppress it relative to pair condensation.
- [47] S. Conti, A. Perali, F. M. Peeters, and D. Neilson, Multicomponent screening and superfluidity in gapped electron-hole double bilayer graphene with realistic bands, *Phys. Rev. B* **99**, 144517 (2019).
- [48] H. A. Fertig, Energy spectrum of a layered system in a strong magnetic field, *Phys. Rev. B* **40**, 1087 (1989).
- [49] M. M. Fogler, L. V. Butov, and K. S. Novoselov, High-temperature superfluidity with indirect excitons in van der waals heterostructures, *Nature Communications* **5**, 4555 (2014).
- [50] J. Toulouse and C. J. Umrigar, Optimization of quantum monte carlo wave functions by energy minimization, *J. Chem. Phys.* **126**, 084102 (2007).
- [51] C. J. Umrigar, J. Toulouse, C. Filippi, S. Sorella, and R. G. Hennig, Alleviation of the fermion-sign problem by optimization of many-body wave functions, *Phys. Rev. Lett.* **98**, 110201 (2007).
- [52] S. Sorella, M. Casula, and D. Rocca, Weak binding between two aromatic rings: Feeling the van der waals attraction by quantum monte carlo methods, *J. Chem. Phys.* **127**, 014105 (2007), <https://doi.org/10.1063/1.2746035>.
- [53] T. Kato, On the eigenfunctions of many-particle systems in quantum mechanics, *Communications on Pure and Applied Mathematics* **10**, 151 (1957).
- [54] N. D. Drummond, R. J. Needs, A. Sorouri, and W. M. C. Foulkes, Finite-size errors in continuum quantum monte carlo calculations, *Phys. Rev. B* **78**, 125106 (2008).
- [55] A. D. Meyertholen and M. M. Fogler, Biexcitons in two-dimensional systems with spatially separated electrons and holes, *Phys. Rev. B* **78**, 235307 (2008).
- [56] R. M. Lee, N. D. Drummond, and R. J. Needs, Exciton-exciton interaction and biexciton formation in bilayer systems, *Phys. Rev. B* **79**, 125308 (2009).

Quadriexcitons and excitonic condensate in a symmetric electron-hole bilayer with valley degeneracy: Supplemental Material

Stefania De Palo,^{1,2,*} F. Tramonto,^{2,†} Saverio Moroni,^{1,3,‡} and Gaetano Senatore^{2,§}

¹CNR-IOM-DEMOCRITOS, Trieste, Italy

²Dipartimento di Fisica, Università di Trieste, strada Costiera 11, 34151 Trieste, Italy

³SISSA (International School for Advanced Studies), via Bonomea 265, 34136 Trieste, Italy

This Supplemental Material contains information on (i) details of the simulations, (ii) optimization of the wave function across a phase boundary, (iii) estimate of the condensate fraction, and (iv) structure of the quadriexcitons. Unless otherwise specified, energies are in Ry^* and distances in a_B^* .

DETAILS OF THE SIMULATIONS

The calculations presented in the main text have been done with $N = 168$ particles [S1] in periodic boundary conditions. The DMC energies, used to map the phase diagram, are calculated with a number of walkers $N_W = 440$ and a time step τ tuned to achieve about 90% acceptance rate for global moves. The biases due to finite N , N_W and τ , estimated in a few representative cases, are all negligible for our purposes, as we show below.

Time step error

The criterion of 90% acceptance rate for the choice of τ affords a rather uniform accuracy across various densities, inter-layer distances, and phases, without the computational burden of explicit extrapolations to zero time step. We have verified in selected cases, some of which are shown in Fig. S1, that

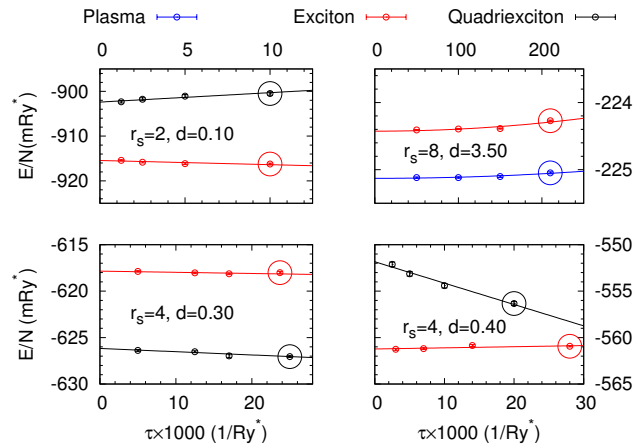


FIG. S1. Dependence of the DMC energy on the time step τ for various phases at selected points of the phase diagram, as specified in the body of each panel.

the time step bias incurred by this choice does not affect our phase diagram in a significant way.

We address in detail the more problematic case we encountered, the exciton-quadriexciton transition at $r_s = 4$ between $d = 0.3$ and $d = 0.4$, inferred from the data shown in the lower panels of Fig. S1. In particular, the energy of the quadriexciton phase at $d = 0.4$ (black symbols in the bottom right panel) has an unusually large time step error of nearly 5mRy^* . The phase boundary is defined as the zero of the linear interpolation between $d = 0.3$ and $d = 0.4$ of the energy difference between the two phases, $\Delta e(d) \equiv (E_{\text{exc}}(d) - E_{\text{qua}}(d))/N$. The data taken at 90% acceptance rate, marked by circles, yield an energy difference (in mRy^*) $\Delta e(0.3) = 9.0$ and $\Delta e(0.4) = -5.1$, while the extrapolations at $\tau = 0$ yield $\Delta e(0.3) = 8.3$ and $\Delta e(0.4) = -9.4$, all with statistical uncertainties of 0.3 or less. The effect of the time step extrapolation is a downward shift of the boundary by no more than 0.02, which would be barely visible on the phase diagram shown in the main text.

Finite size error

Finite-size shell effects in the plasma phase are reduced by subtracting the ideal gas finite-size correction. Smooth finite size effects, with a leading correction[S2] proportional to $N^{-5/4}$, are expected to be similar for the various phases, and to cancel out to a large extent in the energy differences used to map the phase diagram. This is verified in Fig. S2, where we show explicit size extrapolations to the thermodynamic limit of DMC energies in selected cases near phase boundaries. The finite size error at $N = 168$ is few mRy^* for the energy of any given phase, and a fraction of mRy^* for the energy difference between phases. Its effect on the phase diagram is completely negligible.

Population control bias

The number of walkers in our DMC simulations is $N_W = 440$. The population control bias a fraction of mRy^* for the energy of a given phase, and even smaller for the energy difference between phases, as shown in the extrapolation to $1/N_W \rightarrow \infty$ illustrated in Fig. S3. Again, its effect on the phase diagram is completely negligible.

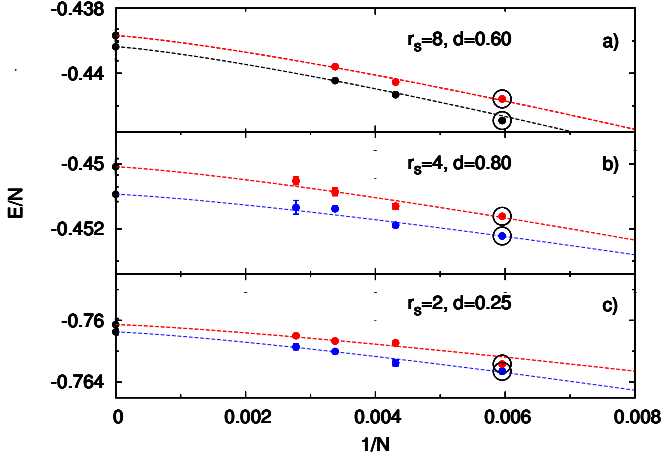


FIG. S2. Dependence of the DMC energy of various phases on the number of particles N , at selected points of the phase diagram specified in the body of each panel. Blue, red and black symbols refer to the plasma, exciton and quadriexciton phase, respectively (the color code does not apply to the extrapolated values, shown in black for all phases). For the plasma phase, the ideal gas finite-size correction has been subtracted. The data used in the main text, corresponding to $N = 168$, are circled. The other system size considered are $N=232$ and 296 . In panels b) and c) we add data for $N = 320$ because they involve the plasma phase whose size extrapolation may be more problematic due to residual shell effects. All energies are extrapolated to zero time step.

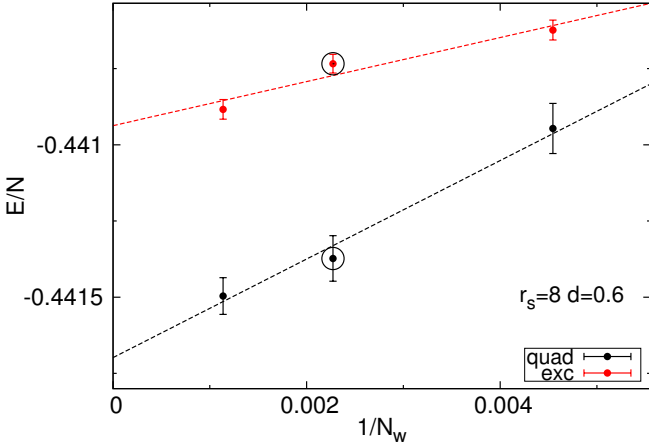


FIG. S3. Extrapolation of the DMC energy to infinite number of walkers for the exciton and quadriexciton phases at $r_s = 8$, $d = 0.6$. The data used in the main text are circled.

OPTIMIZING ACROSS PHASE BOUNDARIES, AND MAPPING THE PHASE DIAGRAM

The functional form of our wave function has the flexibility to represent the quadriexciton, the exciton, and in principle the plasma phases (although for the latter we use in practice a Slater determinant, to which the s -wave pairing function reduces as the Fourier transform of the pair orbital approaches

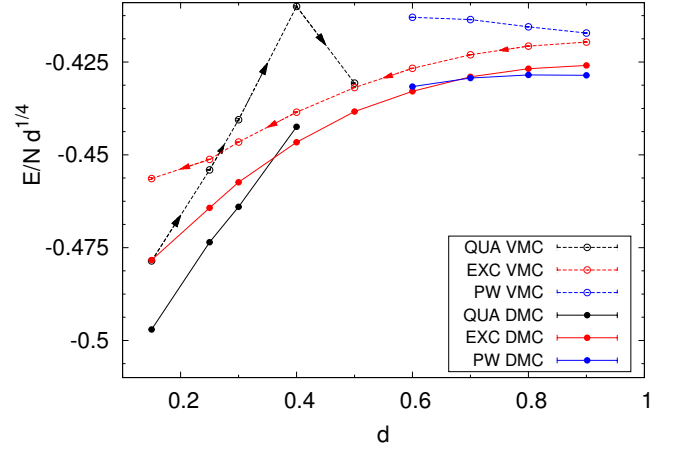


FIG. S4. Energy as a function of the interlayer distance d for the plasma (blue), exciton (red) and quadriexciton (black) phases at $r_s = 4$, calculated with VMC (open circles, dashed lines) and DMC (filled circles, solid lines). The arrows indicate the direction of the optimization series (see text).

the Heaviside function $H(k_F - |k|)$.

An example is shown in Fig. S4, where the empty circles joined by dashed lines show the VMC energies at $r_s = 4$ as a function of d . The black symbols represent a series of optimizations with increasing values of d , as indicated by the arrows, starting in the quadriexcitonic phase at $d = 0.15$. The phase, inferred from structural properties as detailed in the main text and in the last section of this Supplemental Material, remains quadriexcitonic even for $d = 0.3$ and $d = 0.4$, where the VMC energy of the exciton is lower. Eventually, for $d = 0.5$, the phase collapses into excitons. The reverse optimization series, starting in the excitonic phase at $d = 0.9$ and shown by the red symbols, features a similar resilience against phase change around $d \lesssim 0.2$. The optimization series for the plasma phase (blue symbols) has no arrows because, as mentioned, it is done with a different functional form. In this case, the persistence of a metastable phase is trivial.

For reference, the energies displayed in Fig. S4 are listed in Table S1.

These results expose a potentially severe ambiguity in mapping the phase diagram on the basis of structural properties along a directional optimization series. In the example of Fig. S4, the quadriexciton-exciton boundary would be estimated at $d > 0.4$ starting from the quadriexciton and $d < 0.15$ starting from the exciton. A better criterion is to pick the phase with lower variational energy. For the phase diagram presented in the main text we used our best variational upper bounds to the exact ground state energies, given by the DMC results. In Fig. S4, the range of stability of the excitonic phase estimated from VMC energies, d from 0.27 to over 0.9, is about twice as large than our best result, based on DMC energies.

TABLE S1. VMC and DMC energy per particle $E/N(d)$ at $r_s = 4$ for the plasma phase (PW), the excitonic phase (EXC) and the quadriexcitonic phase (QUA) for various distances. DMC simulations are for $N = 168$ total particles, $N_w = 440$ walkers and the time steps are to give an acceptance rate of approximately 90%.

| d | QUA | | EXC | | PW | |
|------|------------|------------|-------------|-------------|-------------|-------------|
| | VMC | DMC | VMC | DMC | VMC | DMC |
| 0.15 | -0.7690(2) | -0.7987(2) | -0.7333(4) | -0.7687(3) | — | — |
| 0.25 | -0.6421(2) | -0.6270(2) | -0.63812(6) | -0.6566(2) | — | — |
| 0.3 | -0.5953(4) | -0.6270(2) | -0.60340(6) | -0.6180(1) | — | — |
| 0.4 | -0.5156(2) | -0.5563(2) | -0.5514(2) | -0.56156(4) | — | — |
| 0.5 | — | — | -0.51358(4) | -0.52127(3) | — | — |
| 0.6 | — | — | -0.48481(3) | -0.49185(2) | -0.46922(7) | -0.49041(7) |
| 0.7 | — | — | -0.46251(1) | -0.46898(4) | -0.45212(7) | -0.46935(7) |
| 0.8 | — | — | -0.44485(3) | -0.45115(4) | -0.43935(4) | -0.45306(5) |
| 0.9 | — | — | — | — | -0.42832(3) | -0.44002(4) |

CONDENSATE FRACTION

The pair condensate in the exciton and quadriexciton phases is defined, following Ref. S3, as the large- r limit of the projected two-body density matrix

$$h_\sigma(r) = \frac{1}{N} \int d\mathbf{r}_{e,\sigma} d\mathbf{r}_{h,\sigma} \rho_2(\mathbf{r}_{e,\sigma} + \mathbf{r}, \mathbf{r}_{h,\sigma} + \mathbf{r}; \mathbf{r}_{e,\sigma}, \mathbf{r}_{h,\sigma}) \quad (\text{S1})$$

averaged over the valley-spin index σ , where ρ_2 is the full two-body density matrix. The Monte Carlo estimate of $h_\sigma(r)$ is $N \langle \Psi_T(R'_\sigma) / \Psi_T(R) \rangle_\pi$, where Ψ_T is the trial function, $\langle \cdot \rangle_\pi$ is an average over N -particle configurations R drawn from the probability distribution π , and R'_σ is obtained from R with a random displacement \mathbf{r} of a σ -type electron-hole pair. Average over all σ -type electron-hole pairs and on angles is also implemented. We calculate both the VMC and DMC

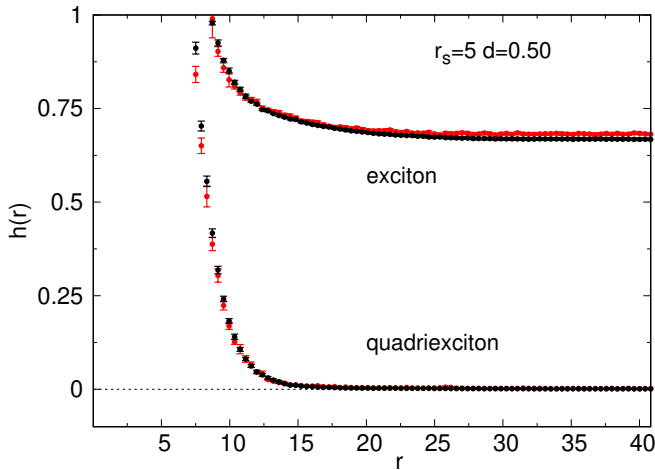


FIG. S5. Mixed (black) and variational (red) estimates of the reduced pair density matrix $h(r)$ for $r_s = 5$ and $d = 0.5$ for the exciton and quadriexciton phases as indicated in the body of the figure.

TABLE S2. Extrapolated estimates [S4] of the condensate fraction n_0/n for selected densities and distances in the region of stability of the excitonic phase. The uncertainty on the estimates is about 3%.

| d | $r_s = 1.5$ | $r_s = 2$ | $r_s = 4$ | $r_s = 5$ | $r_s = 6$ | $r_s = 7$ | $r_s = 8$ |
|------|-------------|-----------|-----------|-----------|-----------|-----------|-----------|
| 0.05 | 0.21 | — | — | — | — | — | — |
| 0.10 | — | 0.23 | — | — | — | — | — |
| 0.15 | — | 0.23 | — | — | — | — | — |
| 0.40 | — | — | 0.54 | — | — | — | — |
| 0.50 | — | — | 0.55 | 0.64 | — | — | — |
| 0.60 | — | — | 0.47 | 0.65 | 0.64 | 0.75 | — |
| 0.70 | — | — | — | 0.63 | — | — | — |
| 0.80 | — | — | — | 0.56 | 0.64 | 0.65 | 0.73 |
| 0.90 | — | — | — | 0.52 | — | — | — |
| 1.00 | — | — | — | 0.48 | 0.57 | 0.61 | 0.63 |
| 1.10 | — | — | — | 0.45 | — | — | — |
| 1.20 | — | — | — | 0.40 | 0.50 | 0.56 | — |
| 1.40 | — | — | — | — | 0.45 | — | 0.53 |
| 1.60 | — | — | — | — | 0.41 | 0.47 | — |
| 1.80 | — | — | — | — | — | — | — |
| 2.00 | — | — | — | — | — | 0.40 | 0.43 |
| 2.50 | — | — | — | — | — | 0.29 | — |
| 2.60 | — | — | — | — | — | — | 0.34 |
| 3.00 | — | — | — | — | — | — | 0.29 |
| 3.25 | — | — | — | — | — | — | 0.24 |

estimates h_{VAR} and h_{MIX} choosing π , respectively, as the variational distribution Ψ^2 and the mixed distribution $\Psi_T \Phi_0$, where Φ_0 is the fixed-node ground state. Our final result is the extrapolated estimate, $h_{\text{EXT}} = 2h_{\text{MIX}} - h_{\text{VAR}}$, which is accurate to higher order in the error of the trial function than either h_{VAR} or h_{MIX} . A small correction from the mixed to the extrapolated estimate is usually supportive of the accuracy

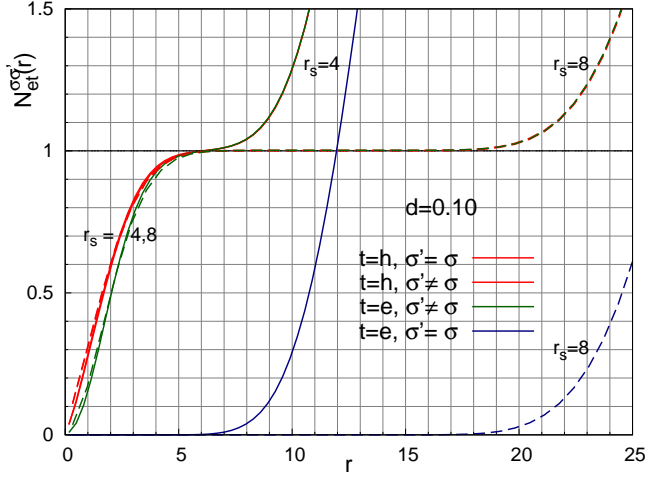


FIG. S6. RCNs (extrapolated estimates), as defined in Eq. S3, at $d = 0.10$ and $r_s = 4$ (full curves), $r_s = 8$ (dashed curves)

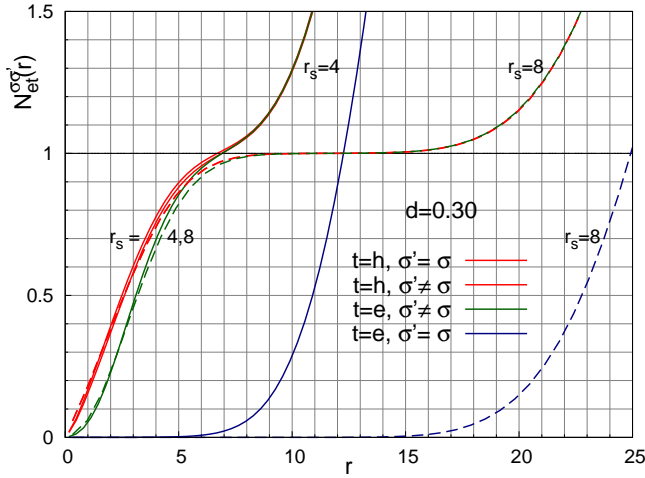


FIG. S7. RCNs (extrapolated estimates), as defined in Eq. S3, at $d = 0.30$ and $r_s = 4$ (full curves), $r_s = 8$ (dashed curves)

of both.

An example of the computed $h(r)$ is shown in Fig. S5 for the excitonic and the quadriexcitonic phases at $r_s = 5$ and $d = 0.5$. For the excitonic phase $h(r)$ is constant, within very small statistical errors, from at least $r = 30$ onwards for both VMC and DMC. This allows us to easily fit the tail of $h(r)$ [S4] and infer an extrapolated estimate of the condensate fraction. For the quadriexcitonic phase the pair condensate fraction is clearly zero. We report extrapolated estimates of the condensate fraction n_0/n for $r_s \leq 8$ in Tab. S2.

QUADRIEXCITON SIZE

The size of quadriexcitons and their arrangement may be partially investigated by looking at pair correlation functions (PCFs) and the ensuing running coordination numbers

(RCNs). The PCF

$$g_{tt'}^{\sigma\sigma'}(s) = \frac{1}{A} \frac{1}{n_{t,\sigma} n_{t',\sigma'}} \left\langle \sum_{i,j}' \delta(\mathbf{s} - \mathbf{r}_{t,\sigma,i} + \mathbf{r}_{t',\sigma',j}) \right\rangle, \quad (\text{S2})$$

provides the probability of finding particles of species (t', σ') at distance s from a particle of the species (t, σ) , with $t = e, h$ a particle type, $\sigma = (v, s_z)$ a valley-spin index, and $n_{t\sigma}$ the areal density of the species (t, σ) . Above $\langle \dots \rangle$ combines the variational (mixed) estimate with the rotational average. The extrapolated estimate for the pair correlation function is $g_{EXT}(s) = 2g_{MIX}(s) - g_{VAR}(s)$. A running coordination number (RCN) may be defined as

$$N_{tt'}^{\sigma\sigma'}(r) = 2\pi n_{t',\sigma'} \int_0^r ds s g_{tt'}^{\sigma\sigma'}(s). \quad (\text{S3})$$

Evidently $N_{tt'}^{\sigma\sigma'}(r)$ provides the distance-dependent pile up of particles of the species (t', σ') around a particle of the species (t, σ) and within a radius r .

In Fig. S6 and S7 we display the electron-electron and electron-hole RCNs in the quadriexcitonic phase for inter-plane distances $d = 0.10$ and $d = 0.30$, respectively, and densities corresponding to $r_s = 4$ and $r_s = 8$. Let's focus on $d = 0.10$ and $r_s = 4$. It is clear that, with $\sigma' \neq \sigma$, $N_{eh}^{\sigma\sigma}(r)$, $N_{eh}^{\sigma\sigma'}(r)$, $N_{ee}^{\sigma\sigma'}(r)$, all increasing functions of r , cross 1 at the same point $r_q \simeq 6$ where $N_{ee}^{\sigma\sigma}(r)$ takes off from 0. In other words, the sphere of radius $r_q = 6$ contains in average exactly 4 electrons and 4 holes (one for each flavour), i.e., a quadriexciton. We shall take r_q as a gross measure of the quadriexciton size, indeed an upper bound to it when $N_{ee}^{\sigma\sigma}(r)$ becomes appreciable only for $r > r_q$. The next quadriexciton, as described by $N_{ee}^{\sigma\sigma}(r)$, appears to be "touching" the one centred at the origin. One may resort to a crude estimate of the average distance r_{qq} between nearest quadriexcitons as

$$r_{qq} = \frac{\int_0^{r_1} ds s^2 g_{ee}^{\sigma\sigma}(s)}{\int_0^{r_1} ds s g_{ee}^{\sigma\sigma}(s)} = 2\pi n_{e,\sigma} \int_0^{r_1} ds s^2 g_{ee}^{\sigma\sigma}(s), \quad (\text{S4})$$

where r_1 is determined by $N_{ee}^{\sigma\sigma}(r_1) = 1$. For $d = 0.10$ and $r_s = 4$ one obtains $r_{qq} \simeq 11$, which appears to be consistent with well defined quadriexcitons; a similar conclusion applies to the case studied in the main text $d = 0.05$, $r_s = 4$, for which $r_q \simeq 5$, while $r_{qq} \simeq 11$. If one considers the case $d = 0.10$, $r_s = 8$ one finds $r_q \simeq 6$ and $r_{qq} \simeq 23$, which is definitively consistent with well defined stable quadriexcitons.

In Fig. S7 we move to a larger interlayer distance $d = 0.30$, which weakens the quadriexciton binding. Indeed at $r_s = 4$ we observe the relaxation to a larger size $r_q = 7$, as compared with $r_q = 6$ found for the $d = 0.10$ case, a minor mixing between neighboring quadriexcitons, and still $r_{qq} \simeq 11$. Lowering the density to $r_s = 8$ we find an appreciable increase in the quadriexciton size, from $r_q = 6$ at $d = 0.1$ to $r_q = 9$, as well as an increase in the distance between quadriexcitons with $r_{qq} \simeq 29$. However at $r_s = 8$ quadriexcitons appear again well separated and thus well defined.

Thus, it would appear that the size r_q of quadriexcitons (i) increases with d , at given r_s , due to the weakening of the binding, and (ii) it may increase with lowering the density (increasing r_s), at given d , if one starts from a situation where there is some mixing between neighboring quadriexcitons. Interestingly, if we extrapolate to $d = 0$ the quadriexciton size calculated for finite d at $r_s = 4$, we find a value comparable to the biexciton size $r_q \simeq 4$ found at $d = 0$ in the one valley system [S5].

* depalo@iom.cnr.it

† Present address: Kyndryl Italia Innovation Services S.r.l., Via

Circonvallazione Idroscalo snc, 20090 Segrate (MI), Italy

‡ moroni@iom.cnr.it

§ senatore@units.it

- [S1] Notice that in the main text N is the number of particle in a layer while here is the number of particles in the bilayer.
- [S2] N. D. Drummond, R. J. Needs, A. Sorouri, and W. M. C. Foulkes, Finite-size errors in continuum quantum monte carlo calculations, *Phys. Rev. B* **78**, 125106 (2008).
- [S3] S. De Palo, F. Rapisarda, and G. Senatore, Excitonic condensation in a symmetric electron-hole bilayer, *Phys. Rev. Lett.* **88**, 206401 (2002).
- [S4] As in Ref. S3, we fit the computed $h(r)$ to $n_0/n + \delta/r^2$ in the tail region $7r_s/\sqrt{2} \leq r \leq 11.5r_s/\sqrt{2} = L/2$, where L is the side of our square simulation box.
- [S5] R. Maezono, P. López Ríos, T. Ogawa, and R. J. Needs, Excitons and biexcitons in symmetric electron-hole bilayers, *Phys. Rev. Lett.* **110**, 216407 (2013).